Chemical Physics Letters 842 (2024) 141205

Contents lists available at ScienceDirect

Chemical Physics Letters

journal homepage: www.elsevier.com/locate/cplett

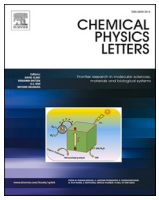

On the conformational shaping of a visible light-driven molecular motor based on barbituric acid in solvents of increasing polarity

Costantino Zazza [a,*], Stefano Borocci [a], Nico Sanna [a,b], Felice Grandinetti [a,c]

[a] Department for Innovation in Biological, Agro-food and Forest Systems, Università della Tuscia (DIBAF), L.go dell'Università, s.n.c., 01100 Viterbo, Italy
[b] CNR-ISTP (Istituto per la Scienza e Tecnologia dei Plasmi), Via G. Amendola 122/D, 70126 Bari, Italy
[c] Istituto per i Sistemi Biologici del CNR (ISB), Sede di Roma - Meccanismi di Reazione c/o Dipartimento di Chimica, Sapienza Università di Roma, P.le A. Moro 5, Rome, Italy

ARTICLE INFO

Keywords:
Artificial nanoscale motors
Supramolecular chemistry
Photochemical properties in nanomaterials

ABSTRACT

A light-driven molecular motor based on barbituric acid is investigated in solvents of increasing polarity by microseconds time scale molecular dynamics and a hybrid quantum mechanical/molecular mechanics approach. Such a synthetic motor is found - in water and methanol - in two different solvent-mediated hydrogen bonding rotamers; on the other hand, in an aprotic solvent like dichloromethane, it systematically features a short-range intramolecular hydrogen bonding contact at room temperature. The observed trend supports the existence of a "lasso" effect modulating photoactive switching in solution. At last, the predicted UV/Vis spectra are found in agreement with experimental measurements.

1. Introduction

The progress of human civilization has always been associated with our ability to assemble machines of increasing complexity and functionalities. For example, some of the machines realized by the genius of Leonardo da Vinci - between the fifteenth and sixteenth centuries - have highlighted the capabilities of some scientists to promote the progress of our species. Clearly, with the advance of time and developments in miniaturization techniques we have observed the appearance of very large "macroscopic" machines - sometimes even distributed on a geographical scale - as well as the advent of "nanoscopic" ones with sizes often confined within single molecular aggregates [1–8]. In analogy with machines of macroscopic sizes or with components of them, a molecular machine is seen as a nanoscale transducer capable of converting external energy coming from different sources (chemical reactions, pH-variation, electrochemical potential, UV–Vis radiation) into quasi-unidimensional mechanical one [9–16]. Some biologically relevant systems like, e.g. ATP synthase [17–19], Titin [20,21] or Myosin [22–24] work efficiently, under physiological conditions, promoting mechanical movements in living organisms converting chemical energy in a fascinating way resembling the behaviour of macroscopic motors and machines. In analogy with biological systems, synthetic molecular motors are capable of controllable directional motions under external stimuli. For example, a prototype for a synthetic chemically driven rotary molecular motor was characterized by T.R. Kelly and co-workers [25]. The original system was made up from a three-bladed triptycene/helicene bond performing a unidirectional 120° rotation activated by a thermally induced isomerization reaction. In the same year, B. Feringa et al. [26] reported about the synthesis of a cyclable and monodirectional rotation, around a central carbon–carbon double bond, in a chiral helical alkene with each 360° rotation involving four discrete isomerization steps activated by UV radiation or by a change in the temperature. In the last two decades, photoactive molecular motors based on *E-Z* isomerization and thermal ratcheting steps have emerged in literature for the development of future-oriented nanotechnological applications.

Taking direct inspiration from literature, we theoretically addressed electrochemically [27–30] and UV–VIS [31,32] driven molecular machines of increasing complexity in different simulation environments. Recently, our attention has turned to molecular systems activated by light due to their reduced environmental impact [33]. In this regard, B. Feringa and co-workers [34] have shown that the visible light can efficiently control - as observed spectroscopically - conformational shaping into a synthetic system composed by an overcrowded alkane-based aggregate featuring barbituric acid in the lower half (see Scheme 1). Interestingly, the authors also addressed the effect of a stereocenter,

* Corresponding author.
E-mail address: costantino.zazza@unitus.it (C. Zazza).

https://doi.org/10.1016/j.cplett.2024.141205
Received 29 December 2023; Received in revised form 11 March 2024; Accepted 12 March 2024
Available online 13 March 2024

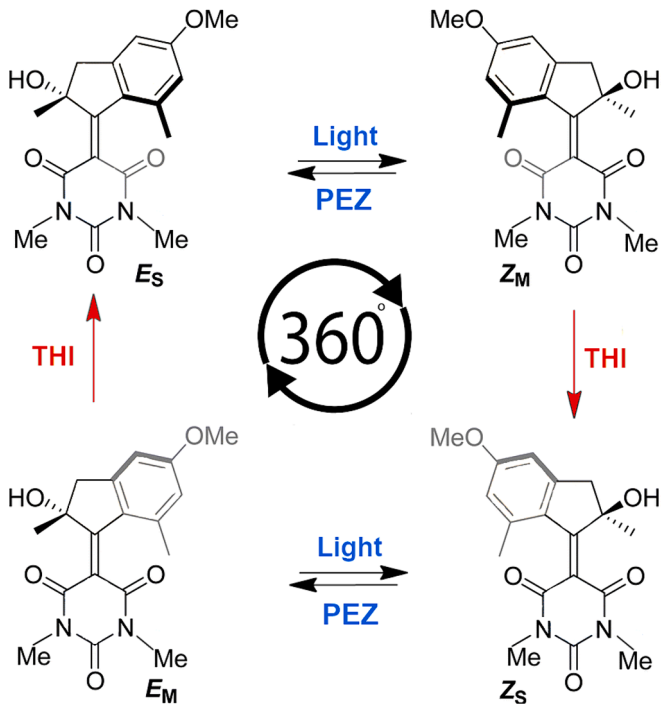

Scheme 1. The proposed controllable rotational cycle of the recently realised UV–VIS driven molecular motor with a lower half based on barbituric acid as proposed in Ref. 34. PEZ stands for Photochemical E–Z isomerisation process while THI for Thermal Helix Inversion.

featuring a tertiary alcohol in the overcrowded moiety in electrostatic interaction with the carbonyl groups of the barbituric acid half, on both mechanical responses in solvent of increasing polarity and isomerization quantum yields (with the latter properties compared with typical second-order generation motors). In this respect, computational simulations while predicting an excited state "lasso" mechanism, in which intra-molecular electrostatic effects drive the rotational cycle of a UV-VIS driven motor, shed some insights on the competitive process between TEZI and THI pathways (see Scheme 1) in gas-phase and in water solution. Excited state molecular dynamics simulations on hundreds of femtoseconds time scale clearly showed that a conical intersection (CInt), characterized by a dihedral angle of rotation along the double bond of ~ 90°, can effectively modulate the formation of the $\boldsymbol{Z_m}$ metastable state versus the return to $\boldsymbol{E_s}$ stable form [34].

Based on previous successful investigations, we report here a computational study on the previously cited artificial UV–VIS driven molecular motor based on barbituric acid [34] in three different solvents (water, methanol and dichloromethane). More specifically, we combined Quantum-Mechanics (QM) and classical Molecular Dynamics (MD) techniques so to address, at atomistic level, the effects of dilute-solvent based environments on the UV–VIS spectroscopic responses and conformationally accessible patterns at room temperature. In agreement with the picture presented in literature [34], our investigation shows that solvation effects can subtly tune the intramolecular supramolecular contacts between the stereocenter and the lower half moiety. Microseconds time scale MD simulations in polar solvents like water and methanol would seem to suggest that – under equilibrium conditions - solvation effects coupled with thermal fluctuations might efficiently activate an intriguing H-bonding switching mechanism in which the proton of the tertiary alcohol may or not be found in interaction with the carbonyl groups of the barbituric acid subunit. On the other hand, in dichloromethane dilute solution the intramolecular [(tertiary alcohol) O-H — O = C (barbituric acid)] H-bonding motif systematically occurs even in the presence of thermal effects. These results *de-facto* support the trend that the rotational cycle depicted in Scheme 1 results more efficient in apolar solvents that typically do not disrupt intramolecular electrostatic contacts in supramolecular aggregates. We then observe an intricate balance between environmental effects and conformational shaping and this balance is highly sensitive to the strength of rotor–solvent interactions. Finally, the estimated spectroscopic parameters (UV-VIS and ^{1}H NMR) in agreement with those obtained in the laboratory give confidence in the convergence of QM/MM approaches when coupled with long time-scale all-atoms MD simulations.

2. Computational details

The molecular systems depicted in Fig. 1 (stable state, $\boldsymbol{E_s}$) were optimized at DFT level adopting the popular hybrid exchange–correlation Becke 3-parameters Lee–Yang–Parr (B3LYP) functional [35–38], its Coulomb-attenuated formulation (Cam-B3LYP) [39] and the PBE0 functional mixing the Perdew–Burke-Ernzerhof (PBE) exchange energy and Hartree–Fock (HF) exchange energy in a set 3:1 ratio, along with the full PBE correlation energy [40]. We used the 6–311+G** basis set [41] for all the atoms and the Grimme's dispersion with the original D3 damping function [42]. The investigated molecular motor was primarily relaxed in gas-phase and subsequently in solution mimicking the hosting dilute solution environment by the Conductor-like Polarizable Continuum Model (C-PCM) [43]. In this respect, we started from the X-ray data available in the literature [34], and considered such a rotor in three different solvents of increasing polarity (namely water, methanol and dichloromethane). In addition, the optimized geometries are also characterized in terms of Normal Modes Analysis (NMA). The calculations were performed with the Gaussian 16 code (Rev. C01) [44].

We then turned attention on the conformational shaping adopted by the artificial molecular rotor in H_2O, CH_3OH and CH_2Cl_2 dilute solutions at room temperature; to this end, for each solvent mentioned a microseconds time-scale MD simulation at 298 K in an NVT ensemble was carried out considering the rotor in the optimized geometry previously extracted from C-PCM based computations [43]. Each MD sampling was started considering the synthetic device at the centre of a cubic box of 44 Å; afterwards, water molecules were introduced in the simulation box using the Single Point Charge (SPC/E) model [45] while for the organic solvents (i.e., methanol and dichloromethane) we used the classical parameters proposed by Van der Spoel and co-workers [46]. At first, in line with the available X-ray data [34], we started the MD simulations

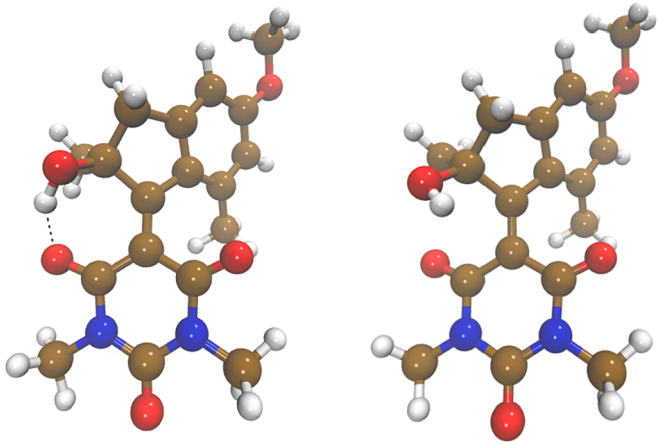

Fig. 1. Geometrical structures of the two HO-rotational isomers ($\boldsymbol{E_s}$ state) of the investigated UV–VIS driven motor based on barbituric acid: left panel, A-type conformation showing the intramolecular O-H—O = C H-bond motif; right panel: B-type conformation. The structures depicted are extracted from optimized geometries at PBE0(D3)/6–311+G** level in water dilute solution simulated by using the C-PCM implicit model.

with the tertiary alcohol interacting - via an intramolecular H-bond contact, with a carbonyl group of the barbituric moiety. The OPLS All-Atom Force Field parameters [47] were adopted for the rotor and MD simulations were performed using GROMACS Software (release 2022.6) [48].

Furthermore, in order to refine - from a dynamical point of view - the lowest valence UV -Vis absorption band experimentally detected at room temperature in different solvents in the range [425.0 nm (penthane) – 444.0 nm (water), see Table 1 in ref. 34 for further details], we have used a Time-Dependent (TD) approach [49] over a QM/MM/C-PCM partitioning scheme as already applied over light-triggered molecular machines [32,33]. In practice, we considered a spherical cavity with a radius of 20 Å with the origin centred over the geometrical centre of the QM region, namely the artificial motor; subsequently, we extracted from an MD trajectory of 400 ns a snapshot every 16.0 ns, corresponding to 25 evenly spaced configurations. The rotor results then confined within 25 different spherical nanodroplets in interaction with the solvent treated both by explicit molecules (treated as atomic point charges) [45,46] and implicit ones (i.e., a spherical C-PCM cavity). In this context, water and dichloromethane are the solvents with the largest difference in terms of dielectric constants [water ($\varepsilon = 78.35$); methanol ($\varepsilon = 32.61$); dichloromethane ($\varepsilon = 8.93$)]. Moreover, following the results obtained analyzing the conformationally accessible phase space in solution via microseconds time-scale MD@298 K, we have considered the synthetic rotor in water in two different conformations (hereafter termed as "A" and "B") featuring or not the presence of the intramolecular H-bond (Fig. 1, left panel). We also remark that position restraints – with a force constant of 10^5 kJ·mol^{-1}·nm^{-2} - are applied on each of the rotor atoms so as to rule out solute dynamics effects. A subset of water molecules forming H-bond contacts with the synthetic solute along the sampling are also treated at QM level (see Fig. 2); these molecules are those found in electrostatic interaction with the donor/acceptor H-bond sites of the rotor on the basis of the geometrical criteria imposed with the gmx hbond module implemented in the GROMACS Software [48]. The H-bond interactions are essentially based on two cutoffs: *i)* the Acceptor-Donor-Hydrogen (Ac–Dn–H) angle between the three atoms involved in the H-bond; *j)* the distance between the two heavy atoms involved in the interaction (Ac–Dn). The applied criteria by default are: Ac–Dn–H angle $\leq 30°$ and Ac–Dn distance ≤ 3.5 Å. On the other hand, in CH_2Cl_2 dilute solution we considered only "A"-like conformations since nanosolvation patterns and thermal effects do not break down the electrostatic glue connecting the stereocenter with the lower half.

3. Results and discussion

The structures of the stable $\boldsymbol{E_s}$ form of the investigated rotor in water, methanol and dichloromethane dilute solution confirm the existence of an intramolecular H-bond between the stereocenter and the carbonyl group of the acid barbituric moiety. The applied DFT functionals show only very small changes in the optimized structural parameters (<3%). As for the low-lying vertical excitations (data summarized in Table 1), the PBE0 functional provides data closer to the experimental findings [34]. As a matter of fact, in water dilute solution, at C-PCM/PBE0(D3)/6–311+G** level of theory, the diagnostic band detected at around 444.0 nm results well reproduced with a value falling at 442.7 nm (oscillator strength, f = 0.41). The other functionals underestimate such a reference spectroscopic data, providing values lying at 416.4 nm (f = 0.55, B3LYP) and 380.4 nm (f = 0.60, Cam-B3LYP). Moreover, our computations indicate that such an absorption band mirrors a valence $^1\pi \rightarrow \pi^*$ character involving HOMO → LUMO orbitals. Furthermore, taking into consideration the metastable species ($\boldsymbol{E_m}$, see Scheme 1), all the applied DFT functional predict – in line with experiments as depicted in Table 1, a valence $^1\pi \rightarrow \pi^*$ red-shifted absorption band: at C-PCM/B3LYP(D3)/6–311+G** level, its peculiar absorption band is estimated falling at 441.5 nm (f = 0.56); the Cam-B3LYP predicts a value lying at 414.4 nm (f = 0.68) and the PBE0 at 467.3 nm (f = 0.39). Calculated electronic spectra for both $\boldsymbol{E_s}$ and $\boldsymbol{E_m}$ isomers are shown in Fig. 3; the main photoreceptive signals between 300 and 800 nm mirrors a valence $^1\pi \rightarrow \pi^*$ character. The π^* molecular orbital features a nodal plane allowing photo-isomerization along the C = C double bond connecting the barbituric acid moiety with the upper asymmetric unit. Experiments had unequivocally shown that, the photo-induced $E \rightarrow Z$ isomerization (from stable $\boldsymbol{E_s}$ to metastable $\boldsymbol{Z_m}$) can be efficiently obtained by exhaustive irradiation of the $\boldsymbol{E_s}$ isomer with visible light at 400 nm; our data then results in qualitative agreement with the transient spectroscopic behaviour and the related solvatocromic red-shift observed when passing from stable/metastable forms [34]. At last, by comparing the minimum energy conformations of the metastable and stable forms, the DFT-predicted ^{1}H NMR chemical shift undergoes – in methanol at C-PCM/PBE0 level - a shift of − 0.09 ppm in line with the measured downfield of − 0.11 ppm (from 1.62 ppm to 1.51 ppm)[34] upon *in situ* irradiation with 420 nm light.

We then extended the modelling considering such a rotor in a classical simulation box (see section 2) so to address the effects of thermal fluctuations and solvation shells on the intramolecular H-bond described before and responsible for the fascinating "lasso" effects pulling the system towards the formation of metastable isomers (see Scheme 1) [34]. We have thus performed 1 microseconds time scale MD simulation considering the stable $\boldsymbol{E_s}$ form in H_2O, CH_3OH and CH_2Cl_2 dilute solutions at 298 K over a time of 3 microseconds under equilibrium conditions. The emerging picture (see Fig. 4) reinforces the idea that, a complex balance of supramolecular contacts modulated by thermal and electrostatic effects play a key role in distinguishing structural and dynamical properties of the investigated device. More specifically, in the upper panel we report the normalized distribution of the dihedral angle characterizing the mutual position of the polar hydrogen within the stereocenter.

The profiles observed in H_2O and CH_3OH feature a bimodal distribution with a peak centred at around −170 degrees and a second peak at −80 degrees: *i)* the first peak is associated with structures of the rotor featuring a short-range H-bond contact [see also the normalized distribution of the (stereocenter-)O-H——O = C(-barbituric acid) in the lower panel of the same figure] between the tertiary alcohol and the carbonyl group of the lower half (i.e., "A"-type conformations); *ii)* the second peak at around −80 degrees instead points to "B"-type structures in which the hydrogen atom of the tertiary alcohol preferentially interacts with surrounding solvent molecules along the sampling. In the polar water and methanol, the investigated rotor dynamically fluctuates between "A" and "B" type conformations. In addition, in water the "B"-type rotamer results statistically preferred (at least within the explored time range of 1 μs) with respect to the other one. The Helmholtz's free energy change profile (ΔA_c) during the MD sampling in the NVT ensemble - i.e. $\Delta A_c = -k_bT \ln [\rho(\varphi_{H\text{-}O\text{-}C\text{-}C})/\ \rho(\varphi^*_{H\text{-}O\text{-}C\text{-}C})]$, where: k_b stands

Table 1
Computed absorption parameters - at TD-DFT/(D3)/6–311+G** level of theory - for the investigated rotor in water dilute solution modelled via C-PCM algorithm (see Section 2). The molar absorption coefficients (Ɛ) are estimated according to Gaussum Software [50].

System	Level	λ_{max} (nm)	ε ($M^{-1}cm^{-1}$)
$\boldsymbol{E_s}$ isomer	Exp (Ref. 34)	444	12 800
$\boldsymbol{E_s}$ isomer	TD/PBE0	443	30 434
$\boldsymbol{E_s}$ isomer	TD/B3LYP	416	39 567
$\boldsymbol{E_s}$ isomer	TD/Cam-B3LYP	380	47 127
$\boldsymbol{E_m}$ metastable	Exp (Ref. 34, from ΔA*)	492	
$\boldsymbol{E_m}$ metastable	TD/PBE0	467	30 910
$\boldsymbol{E_m}$ metastable	TD/B3LYP	441	40 971
$\boldsymbol{E_m}$ metastable	TD/Cam-B3LYP	414	44 823

*From nanosecond transient absorption of $\boldsymbol{E_s}$ in water at room temperature upon irradiation at 425 nm, see Figure S23 in the Electronic Supporting Information (ESI) of Ref. 34.

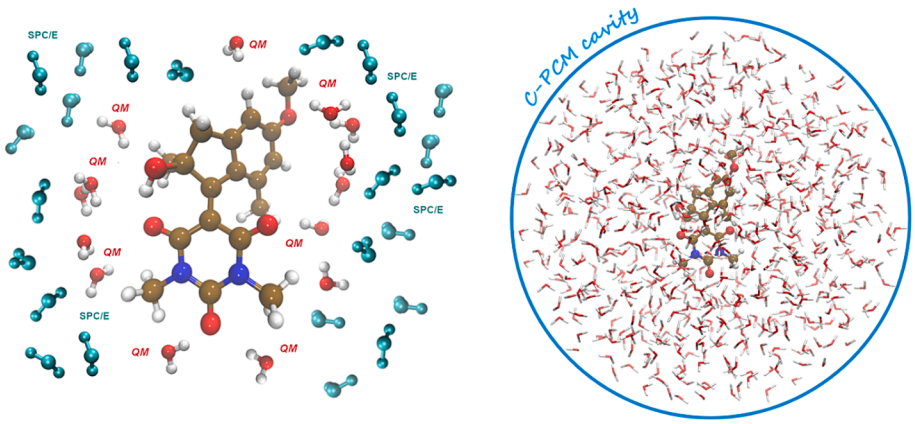

Fig. 2. Left panel: the UV–VIS driven motor (E_s state) - at C-PCM/PBE0(D3)/6–311+G** level (Conf-A) - with a subset of solvent molecules forming the nearest solvation shell as extracted from a MD simulation in water solution in which encircling water molecules are treated both at QM [PBE0(D3)/6–311+G**] level and MD level (atomic point charges) on the basis of their interactions with donor/acceptor H-bond sites of the rotor; in this respect, water molecules selected within the QM layer are those forming H-bonds with the solute according to the "gmx hbond" application within the Gromacs software [48]. Right panel: a spherical QM/MM/C-PCM aqueous nanodroplet with a radius of 20 Å hosting the investigated rotor (see Section 2).

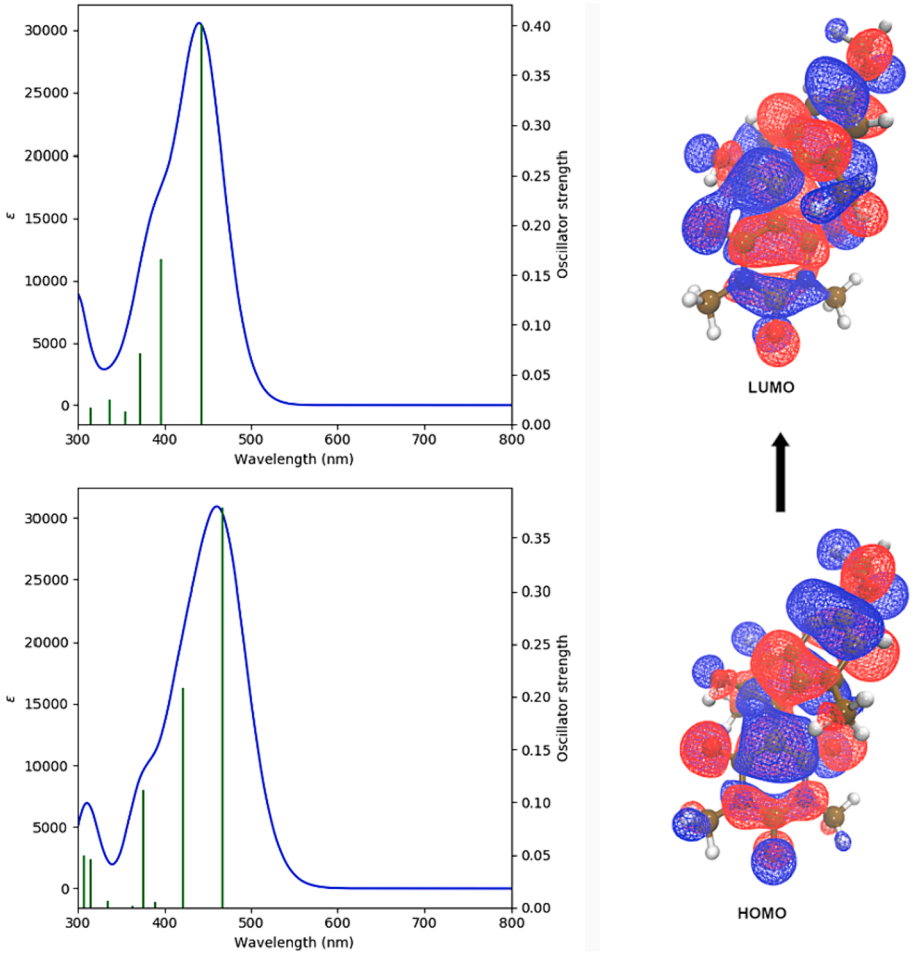

Fig. 3. Upper-left panel: UV-Vis absorption spectra (Ɛ in $L \cdot mol^{-1} \cdot cm^{-1}$) from stable $\boldsymbol{E_s}$ isomer at C-PCM/PBE0(D3)/6–311+G** level of theory in dilute water environment. Lower-left panel: same spectroscopic data from metastable $\boldsymbol{E_m}$ isomer. The molecular orbitals responsible for the main absorption signal in the range 300–800 nm are also displayed for $\boldsymbol{E_m}$ form. The blue colour reflects the positive (+) counterpart of the corresponding eigenvector and an isodensity surface value of 0.01 $e \cdot Å^3$ is represented.

for the Boltzmann's constant; $\rho(\varphi_{H\text{-}O\text{-}C\text{-}C})$ represents the probability density of finding the dihedral angle at a given $\varphi_{H\text{-}O\text{-}C\text{-}C}$ value while $\varphi^*_{H\text{-}O\text{-}C\text{-}C}$ indicates the reference condition corresponding to the most frequent value in the explored range - reveals that the most stable conformations feature a $\varphi^*_{H\text{-}O\text{-}C\text{-}C}$=~80°; as a consequence, the conf-B conformation is predicted to be thermodynamically more favourable by about + 1.22 kJ/mol if compared with conf-A rotamer. On the other hand, in methanol the rotor tends to favour the formation of the H-bond

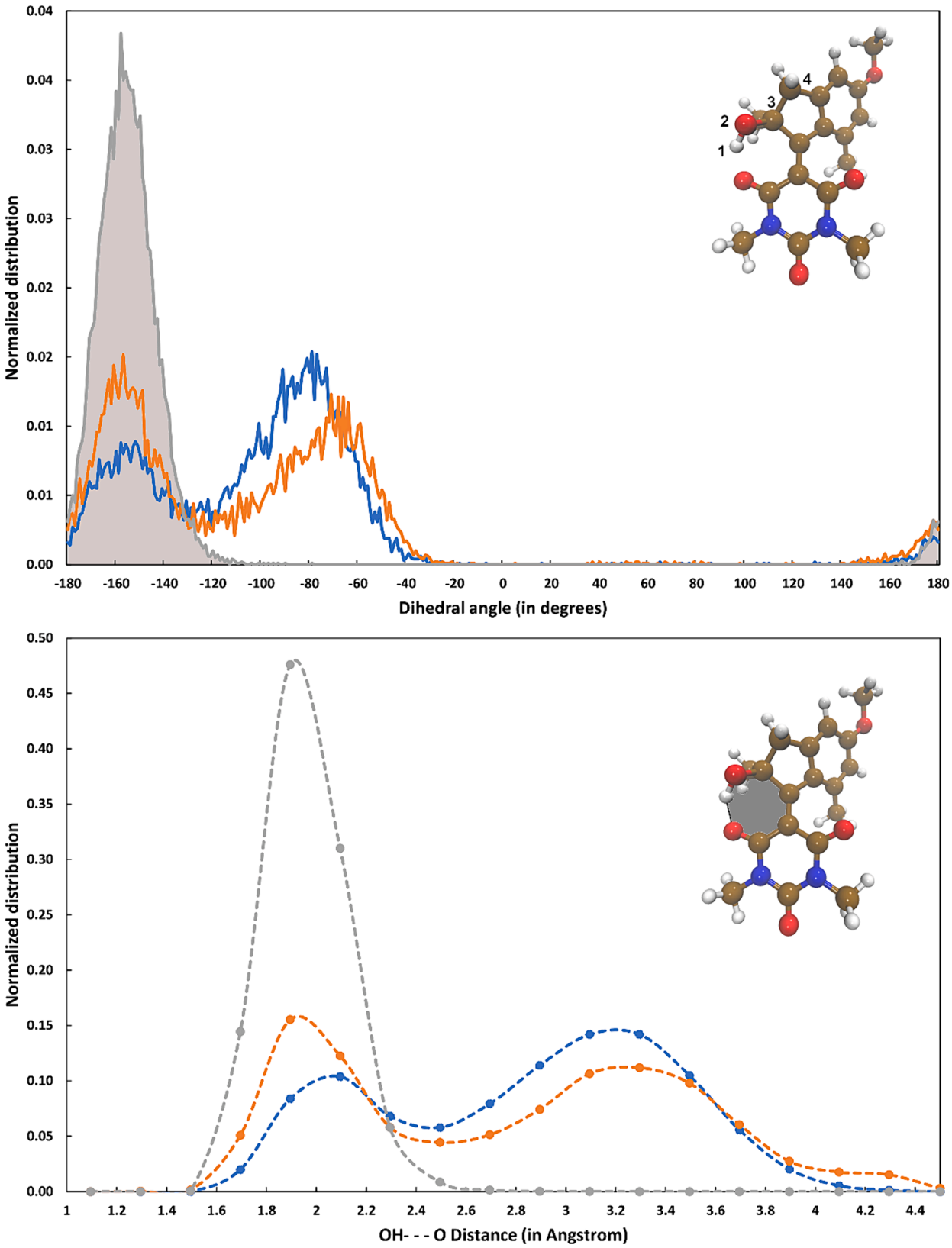

Fig. 4. Upper panel: normalized "H-O-C-C" dihedral angle ($\varphi_{H\text{-}O\text{-}C\text{-}C}$) distribution of the investigated UV–VIS driven $\boldsymbol{E_s}$ molecular motor in water (blue colour), methanol (orange) and dichloromethane (grey) dilute solution estimated by using a microseconds time scale classical MD sampling in NVT ensemble (see section 2) at 298 K. Lower panel: Normalized distribution of the OH—O intramolecular H-bonding distances (in Å). Distances shorter than 2.5 Å essentially characterize the presence of the A-type conformations showing the presence of a short-range intramolecular O-H—O = C H-bonding motif. A 0.25 Å spacing is used and the mean value of the O-H——O = C distance within each interval identifies the X-value.

between the stereocenter and the carbonyl group of the barbituric acid, $\Delta A_c(\varphi_{H\text{-}O\text{-}C\text{-}C}{=}{\sim}80^\circ) = +0.66$ kJ/mol. Interestingly, our MD simulations also show that, in dichloromethane, the stable $\boldsymbol{E_s}$ form of the rotor systematically features conformations showing the presence of a stable short-range H-bond intramolecular contact with a maximum at around 2.0 Å (see Fig. 4, lower panel).

The MD sampling in water solution highlights that, almost the 85 % of the time the synthetic solute establishes, along the sampling, at least 5 H-bond contacts with solvent molecules with a maximum of 7 electrostatic contacts; this value decreases to a maximum of 3 contacts only considering the tertiary alcohol moiety and the local carbonyl group as donor/acceptor. In addition, by extending the analysis in methanol - if compared with water – our simulations display a lower hydrogen bonding formation ability; as a matter of fact, the computed distribution features a maximum (almost the 27 %) in proximity of 3 H-bond interactions between the whole rotor and the solvent. In this respect, the contribution in terms of electrostatic interactions ascribed to the tertiary alcohol and the local carbonyl group features - on average - a value of 58 % of nanosolvation patterns showing 1 or 2 H-bonds with the hydroxyl group of the solvent. In summary, in line with experimentally observed mechanical responses, our computational investigations based on all-atom MD simulations clearly evidence that thermal effects, coupled with intermolecular hydrogen bonding networks surrounding the rotor, produce a subtle tuning of the conformational shaping under exercise

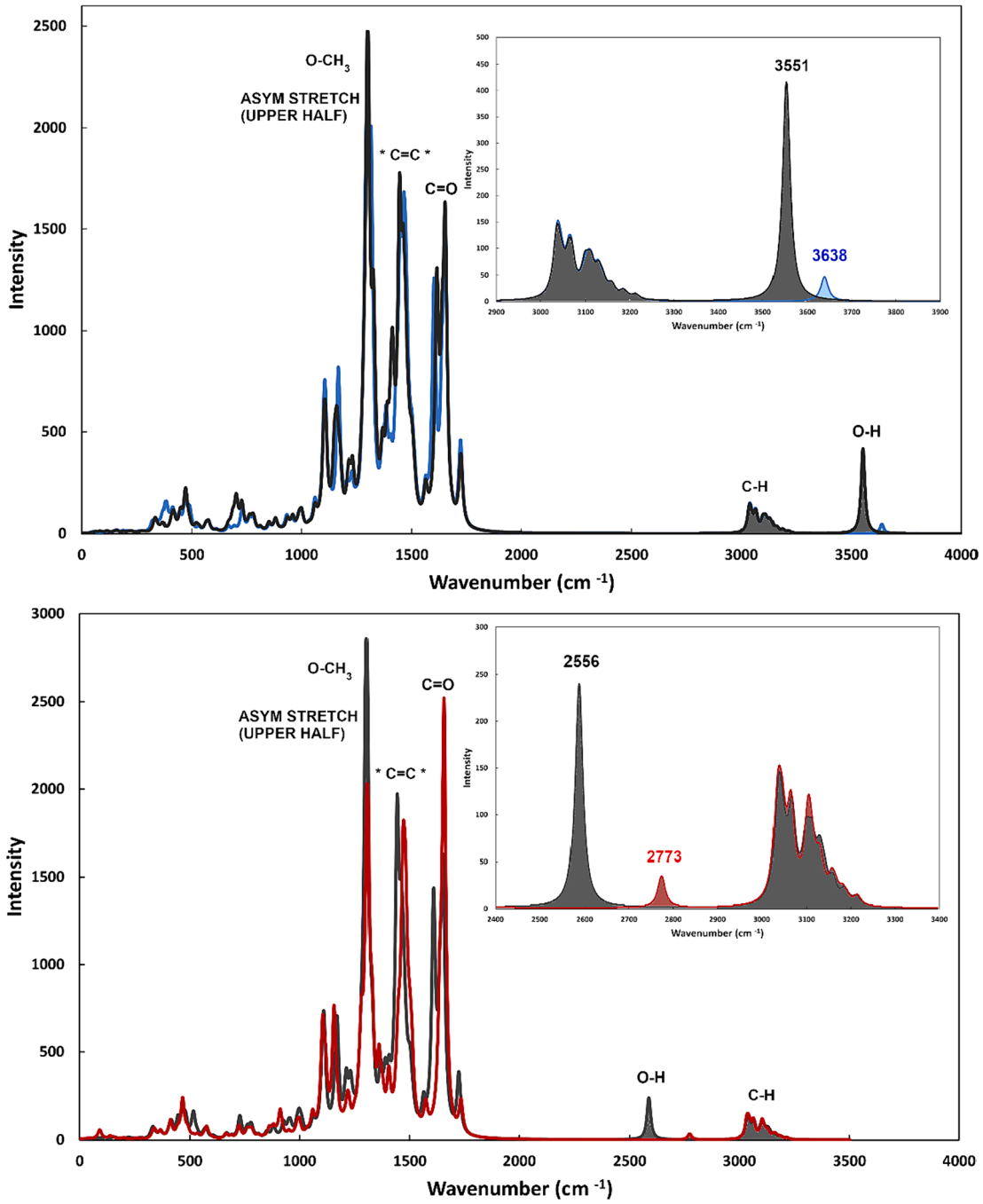

Fig. 5. Computed IR absorption spectra in water for the investigated artificial molecular rotor ($\boldsymbol{E_s}$ form) at C-PCM/B3LYP(D3)/6–311+G** level of theory. Upper panel: A-type conformation featuring a O-H—O = C intramolecular contact is reported using a back solid line while B-type with a blue solid line. Lower panel: A-type with a O-D—O = C contact is reported using a grey solid line; B-type with a red solid line.

conditions. At last, dynamics suggest that at room temperature the investigated rotor in both the protic solvents continuously oscillates between "A" and "B" type conformations. This aspect was also investigated by estimating the IR absorption spectra for both the sampled rotamers and the data displayed in Fig. 5. The local intra-rotor H-bond contact has mainly the effects to modulate the frequency of the stretching mode associated with the proton of the tertiary alcohol. In fact, in the absence of such a supramolecular contact, the stretching mode detected in water occurs at higher frequencies (3638 cm^{-1} *vs* 3551 cm^{-1}) and is accompanied by a reduction in its intensity. Such a displacement is magnified introducing deuterium in the molecular structure; the isotopic effect arising from O-[D/H]——O = C substitution shifts the two signals at lower frequencies being detected at 2556 cm^{-1} and 2773 cm^{-1} (with a spacing of 217 cm^{-1}). These data highlight that conformational changes in this rotor might be most likely revealed addressing isotopic-derived effects in different solvents. In addition, C = O symmetric and asymmetric stretching involving the two chemical groups far from the asymmetric centre result confined around 1720 cm^{-1} and 1650 cm^{-1} for both the forms while the C = O stretching in proximity of the stereocentre undergoes a slight blue shift (from 1600 to 1613 cm^{-1}) as a function of the intramolecular electrostatic contact. Among other things: *i)* the *C=C* stretching along the double bond connecting the two subunits provides a characteristic frequency lying at 1443 cm^{-1} (see Fig. 5); *j)* the prominent peak displayed at around 1300

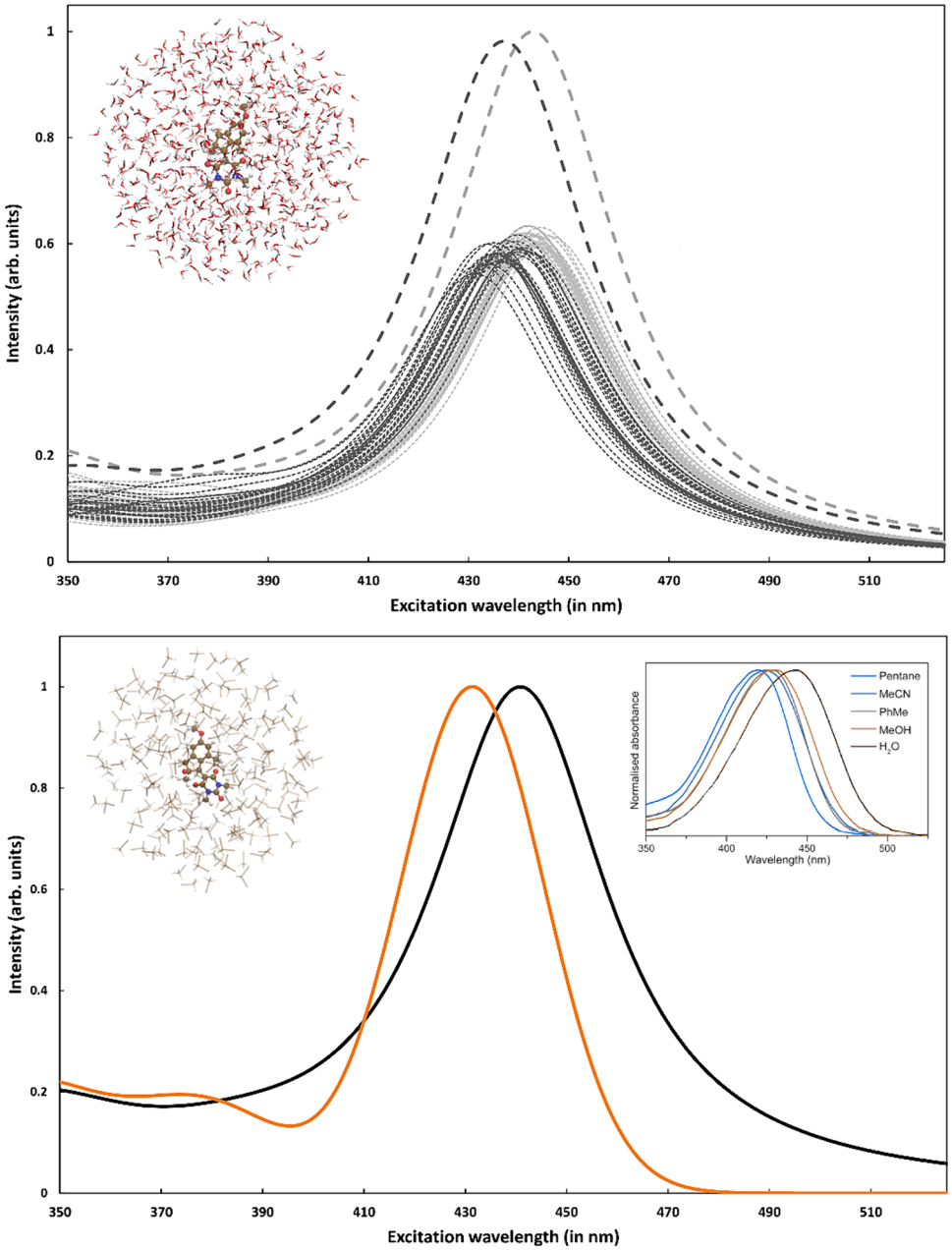

Fig. 6. Upper panel: Normalized UV-Vis absorption band - $\boldsymbol{E_s}$ at [PBE0(D3)/6–311+G**/MM + C-PCM] level - in H_2O. We have considered the rotor in conf-A (grey dashed lines) and conf-B (light-grey dashed lines). The excitations are computed using spherical nanodroplets hosting the molecular motor and surrounded by a C-PCM cavity; water molecules in H-bond contact with the rotor are treated at QM level (see section 2). Lower panel: Normalized UV-Vis absorption band - $\boldsymbol{E_s}$ at [PBE0(D3)/6–311+G**/MM + C-PCM] level - in H_2O (conf-A ⇄ conf-B, black profile) and CH_2Cl_2 (orange profile). The absorption band in water is computed by using 25 (conf-A) + 25(conf-B) MD (400 ns@298 K) frames; it is estimated considering a mixture of the two rotamers, A(37.9 %) + B(62.1 %)-type, with a population ratio derived through the Helmholtz free energy difference ($\Delta A_{B\rightarrow A}$, see section 2) at 298 K of 1.22 kJ/mol. In the inset we show: left side) a QM/MM/C-PCM nanodroplet showing the synthetic rotor in CH_2Cl_2; right side) experimental spectra in different solvents [34].

cm^{-1} is ascribed to the typical stretching mode associated to the ether group in the upper half moiety of the rotor. In this respect, we observe that such an IR band increases its own intensity when close in energy to an asymmetric C-C stretching mode involving the stereocenter.

Furthermore, with the target of theoretically modelling the lowest UV-Vis absorption maximum of $\boldsymbol{E_s}$ form of the rotor detected between 420 and 445 nm in multiple solvents, we introduce a QM/MM/C-PCM partitioning scheme as previously applied over similar systems [32,33] In the QM region, inspired by unconstrained MD simulations (see Figs. 2, 3 and 4), we have properly considered both "A" and "B"-like conformations with structures optimized at C-PCM-PBE0(D3)/6–311+G** level (see Fig. 1). These structures were then embedded within a classical simulation box and a MD trajectory of 400 ns in water at 298 K was sampled for each conformation. Subsequently, the classical MD trajectories have been analyzed extracting an MD snapshot every 16 ns. These uncorrelated 25 + 25 evenly spaced configurations, showing the molecular motor in explicit solvent molecules, are then used to build up nanodroplets with spherical shapes. In this respect, the absorption properties for both the forms of the rotor are obtained by combining QM [PBE0(D3)]/6–311+G**)/MM/C-PCM excitation wavelengths with oscillator strengths and using gaussian broadening functions having a full width at half maximum (FWHM) of 20 nm. The convoluted adsorption signals that have emerged (see Fig. 6, upper panel) show two single peak profiles in the range 350–510 nm with a λ_{max} falling at 445.2 nm (conf-A) and 440.4 nm (conf-B). Interestingly, we observe that when the intramolecular H-bond is present, the rotor features slightly longer excitation wavelengths; the computed QM[PBE0(D3)]/6–311+G**)/MM/C-PCM excitation wavelengths fall in the 440–446 nm range with an average value of 443.9 nm and a standard deviation of 1.3 nm. The corresponding oscillator strengths result as well tuned by solvation effects, spanning values between 0.63 and 0.56 au. Conf-B instead features wavelengths between 432 and 442 nm (average value of 437.1 nm and standard deviation of 2.1 nm) with oscillator strength between 0.61 and 0.53 au. We also report in Fig. 6 (lower panel) a comparison with experimental measurements. To this end, the UV-Vis absorption pathways in water are weighted by using the free energy difference of 1.22 kJ/mol (conf-A ⇄ conf-B, with B-type conformations taken as reference condition) derived by 1 μs of MD sampling. We also display in the same Figure, the UV/Vis absorption band estimated by considering the motor in CH_2Cl_2 solution at 298 K. In this context, the same QM/MM/C-PCM partitioning scheme is applied in CH_2Cl_2 where only the sampled conformer showing the stable intramolecular H-bond is considered in our modelling (see Fig. 4). The only difference is that solvent molecules [46] are not treated at QM level because of the lack of H-bonding interactions with the solute. In water the low-lying valence $^1\pi \rightarrow \pi^*$ absorption band featuring a maximum lying at 442.5 nm meets the experimental assignment at 444.0 nm. Also, in line with the trend experimentally detected in solvent of different polarity, the same absorption result blue shifted in dichloromethane by ~ 11 nm (λ_{max} = 431.3 nm *vs* $\lambda(exp)_{max}$ = 432.0 nm) [34] The proposed simulation scenario then reproduces well the experimental solvatochromic effect highlighting the push–pull character of barbituric acid derivatives.

4. Conclusions

Herein we report a computational study focused on a recently proposed UV–VIS driven artificial molecular rotor based on barbituric acid in dilute solution in the presence of solvents of increasing polarity. Microseconds time scale classical MD sampling have been carried out so to address the conformational flexibility of such a rotor under exercise conditions. The obtained results highlight a strong effect of the environment (solvation patterns coupled with thermal fluctuations) on the conformational shaping adopted by the synthetic rotor in solution. This dependence was already observed by B. Feringa and coworkers while analyzing the photo-induced mechanical responses of the barbituric-derived motor in different contests. Therefore, in line with experimental assumptions, the intramolecular [(stereocenter-)O-H——O = C(-barbituric acid)] interaction is seen to be subtly tuned by environmental conditions. A combined self-consistent QM/MM/C-PCM approach in nanodroplets is also applied - for the first time over microseconds time scale in different environments coupled with thermal effects - to estimate the UV/Vis absorption spectra of the motor in water and dichloromethane. Although we have not considered excited state dynamics and we are far from a full QM approach, we are confident that the present contribution, coupled with previous simulations and experimental evidence can shed some light on the mechanism of action of such an intriguing molecular rotor.

CRediT authorship contribution statement

Costantino Zazza: Writing – original draft, Visualization, Software, Methodology, Investigation, Data curation. **Stefano Borocci:** Visualization, Supervision, Methodology, Conceptualization. **Nico Sanna:** Visualization, Supervision, Project administration. **Felice Grandinetti:** Writing – original draft, Conceptualization.

Declaration of competing interest

The authors declare that they have no known competing financial interests or personal relationships that could have appeared to influence the work reported in this paper.

Data availability

Data will be made available on request.

References

[1] V. Balzani, A. Credi and M. Venturi, Molecular machines and devices: concepts and perspectives for the nanoworld; Wiley-VCH: Weinheim, Germany, 2008. doi: 10.1002/9783527621682.
[2] R.A.L. Jones, Soft machines, nanotechnology and life, Oxford University Press, Oxford, U.K., 2004.
[3] E.R. Kay, D.A. Leigh, F. Zerbetto, Synthetic molecular motors and mechanical machines, Angew. Chem. Int. Ed. 46 (2006) 72–191, https://doi.org/10.1002/anie.200504313.
[4] J.F. Stoddart, The chemistry of the mechanical bond, Chem. Soc. Rev. 38 (2009) 1802–1820, https://doi.org/10.1039/B819333A.
[5] B. Feringa, Nanotechnology: in control of molecular motion, Nature 408 (2000) 151–154, https://doi.org/10.1038/35041665.
[6] S. Silvi, A. Credi, A. Molecular Motors and Machines, In Nanotechnology for Biology and Medicine; Springer: New York, (2012) pp 71−100. doi: 10.1007/978-0-387-31296-5_4.
[7] S. Saha, J. F. Stoddart, Chapter 8 in Molecular Motors and Muscles, Functional Organic Materials: Syntheses, Strategies and Applications, Editor(s): T.J.J. Müller and U.H. F. Bunz, Wiley-VCH Verlag GmbH & Co. KGaA, 2007. doi: 10.1002/9783527610266.ch8.
[8] A.L. Santos, D. Liu, A.K. Reed, A.M. Wyderka, A. van Venrooy, J.T. Li, V.D. Li, M. Misiura, O. Samoylova, J.L. Beckham, C. Ayala-Orozco, A.B. Kolomeisky, L.B. Alemany, A. Oliver, G.P. Tegos, J.M. Tour, Light activated molecular machines are fast-acting broad-spectrum antibacterials that target the membrane, Sci. Adv. 8 (2022), art. no. eabm2055. doi: 10.1126/sciadv.abm2055.
[9] P. Reimann, P. Hänggi, Introduction to the physics of Brownian motors, Appl. Phys. A 75 (2002) 169–178, https://doi.org/10.1007/s003390201331.
[10] D.R. Astumian, Thermodynamics and kinetics of a Brownian motor, Science 276 (1997) 917–922, https://doi.org/10.1126/science.276.5314.917.
[11] V. Balzani, A. Credi, M. Venturi, Molecular Devices and Machines, NanoToday 2, (2007), 18−25 and quoted references therein cited.doi: 10.1016/S1748-0132(07)70055-5.
[12] S. Saha, J.F. Stoddart, Photo-driven molecular devices, Chem. Soc. Rev. 36 (2007) 77–92, https://doi.org/10.1039/B607187B.
[13] A. Livoreil, C.O. Dietrich-Buchecker, J.-P. Sauvage, Electrochemically triggered swinging of a [2]-catenate, J. Am. Chem. Soc. 116 (1994) 9399, https://doi.org/10.1021/ja00099a095.
[14] L. Fang, M.A. Olson, D. Benítez, E. Tkatchouk, W.A. Goddard III; J. F. Stoddart, Mechanically Bonded Macromolecules, Chem. Soc. Rev. 39 (2010) 17−29. doi: 10.1039/B917901A.
[15] J.F. Stoddart, Molecular machines, Acc. Chem. Res. 34 (2001) 410–411, https://doi.org/10.1021/ar010084w.
[16] M. Schliwa, G. Woehlke, Molecular motors, Nature 422 (2003) 759–765, https://doi.org/10.1038/nature01601.

[17] J. Squire, D. Parry, Fibrous Protein: Muscle and Molecular Motors; Advances in Protein Chemistry Series, vol. 71, Academic Press, San Diego, 2005.
[18] H. Hess, G.D. Bachand, Biomolecular motors, Nanotoday 8 (2005) 22, https://doi.org/10.1016/S1369-7021(05)71286-4.
[19] R.K. Nakamoto, J.A. Baylis Scanlon, M.K. Al-Shawi, The rotary mechanism of the ATP synthase, Arch. Biochem. Biophys. 476(2008) 43-50. https://doi:10.1016/j.abb.2008.05.004.
[20] O. Mayans, P.F. van der Ven, M. Wilm, A. Mues, P. Young, D.O. Fürst, M. Wilmanns, M. Gautel, The structural basis of the activation mechanism of the serine kinase domain of the giant muscle protein titin during myofibrillogenesis, Nature 395 (1998) 863, https://doi.org/10.1038/27603.
[21] S. Lv, D.M. Dudek, Y. Cao, M.M. Balamurali, J. Gosline, H. Li, Designed biomaterials to mimic the mechanical properties of muscles, Nature 465 (2010) 69, https://doi.org/10.1038/nature09024.
[22] S. Watanabe, K. Mabuchi, R. Ikebe, M. Ikebe, Mechanoenzymatic characterization of human myosin Vb, Biochem. 45 (2006) 2729, https://doi.org/10.1021/bi051682b.
[23] G. Piazzesi, M. Reconditi, M. Linari, L. Lucii, V. Lombardi, mechanism of force generation by myosin heads in skeletal muscle, Nature 415 (2002) 659–662, https://doi.org/10.1038/415659a.
[24] M. Caremani, M. Marcello, I. Morotti, et al., The force of the myosin motor sets cooperativity in thin filament activation of skeletal muscles, Commun. Biol. 5 (2022) 1266, https://doi.org/10.1038/s42003-022-04184-0.
[25] T. Kelly, H. De Silva, R. Silva, Unidirectional rotary motion in a molecular system, Nature 401 (1999) 150–152, https://doi.org/10.1038/43639.
[26] N. Koumura, R. Zijlstra, R. van Delden, N. Harada, B. Feringa, Light-driven monodirectional molecular rotor, Nature 401 (1999) 152–155, https://doi.org/10.1038/43646.
[27] G. Mancini, C. Zazza, M. Aschi, N. Sanna, Conformational analysis and UV/Vis spectroscopic properties of a rotaxane-based Molecular machine in acetonitrile dilute solution: when simulations meet Experiments, Phys. Chem. Chem. Phys. 13 (2011) 2342–2349, https://doi.org/10.1039/C0CP01773F.
[28] C. Zazza, G. Mancini, G. Brancato, N. Sanna, V. Barone, Neutral Molecular shuttle in acetonitrile dilute solution investigated by Molecular dynamics and density functional theory, Comput. Theor. Chem. 985 (2012) 53–61, https://doi.org/10.1016/j.comptc.2012.01.039.
[29] C. Zazza, A. Amadei, N. Sanna, M. Aschi, Can a synthetic thread act as an electrochemically switchable molecular device? Chem. Commun. 29 (2008) 3399–3401, https://doi.org/10.1039/B804031A.
[30] C. Zazza, G. Mancini, A. Amadei, N. Sanna, M. Aschi, A fast redox-induced switching mechanism in a conformationally controllable Molecular thread in solution, Phys. Chem. Chem. Phys. 12 (2010) 4552–4554, https://doi.org/10.1039/B926627E.
[31] C. Zazza, S. Borocci, N. Sanna, A computational study of a light-driven artificial device: a third generation rotational photo-molecular motor in dilute solutions, Phys. Chem. Chem. Phys. 26 (2024) 5399–5407, https://doi.org/10.1039/D3CP05116A.
[32] C. Zazza, G. Mancini, G. Brancato, V. Barone, In silico study of Molecular-engineered Nanodevices: a lockable light-driven motor in dichloromethane solution, J. Phys. Chem. Lett. 4 (2013) 3885–3890, https://doi.org/10.1021/jz4019404.
[33] C. Zazza, S. Borocci, N. Sanna, A theoretical study of a light-powered artificial molecular motor in dichloromethane solution under equilibrium conditions, Chem. Phys. Lett. 829 (2023) 140758, https://doi.org/10.1016/j.cplett.2023.140758.
[34] K. Kuntze, D.R.S. Pooler, M. Di Donato, M.F. Hilbers, P. Van Der Mulen, W. J. Buma, A. Priimagi, B. Feringa, S. Crespi, A visible-light-driven molecular motor based on barbituric acid, Chem. Sci. 14 (2023) 8458–8465, https://doi.org/10.1039/D3SC03090C.
[35] W. Koch, M. C. Holthausen, A Chemist's Guide to Density Functional Theory, Wiley-VCH Verlag GmbH, 2001. doi: 10.1002/3527600043.
[36] A.D. Becke, Density-functional exchange-energy approximation with correct asymptotic behavior, Phys. Rev. A 38 (1988) 3098, https://doi.org/10.1103/PhysRevA.38.3098.
[37] C. Lee, W. Yang, R.G. Parr, Development of the Colle-Salvetti correlation-energy formula into a functional of the electron density, Phys. Rev. B 37 (1988) 785, https://doi.org/10.1103/PhysRevB.37.785.
[38] S.H. Vosko, L. Wilk, M. Nusair, Accurate spin-dependent electron liquid correlation energies for local spin density calculations: a critical analysis, Can. J. Phys. 58 (1980) 1200, https://doi.org/10.1139/p80-159.
[39] T. Yanai, D. Tew, N. Handy, A new hybrid exchange-correlation functional using the Coulomb-attenuating method (CAM-B3LYP), Chem. Phys. Lett. 393 (2004) 51–57, https://doi.org/10.1016/j.cplett.2004.06.011.
[40] C. Adamo, V. Barone, Toward reliable density functional methods without adjustable parameters: the PBE0 model, J. Chem. Phys. 110 (1999) 6158, https://doi.org/10.1063/1.478522.
[41] T.H. Dunning, P.J. Hay, Gaussian basis sets for Molecular calculations, in: H. F. Schaefer (Ed.), Methods of Electronic Structure Theory. Modern Theoretical Chemistry, vol 3, Springer, Boston, MA, 1977, https://doi.org/10.1007/978-1-4757-0887-5_1.
[42] S. Grimme, J. Antony, S. Ehrlich, H. Krieg, A consistent and accurate ab-initio parameterization of density functional dispersion correction (DFT-D) for the 94 elements H-Pu, J. Chem. Phys. 132 (2010) 154104, https://doi.org/10.1063/1.3382344.
[43] M. Cossi, N. Rega, G. Scalmani, V. Barone, Energies, structures, and electronic properties of molecules in solution with the C-PCM solvation model, J. Comput. Chem. 24 (2003) 669–681, https://doi.org/10.1002/jcc.10189.
[44] Gaussian 16, Revision C.01, M. J. Frisch, G. W. Trucks, H. B. Schlegel, G. E. Scuseria, M. A. Robb, J. R. Cheeseman, G. Scalmani, V. Barone, G. A. Petersson, H. Nakatsuji, X. Li, M. Caricato, A. V. Marenich, J. Bloino, B. G. Janesko, R. Gomperts, B. Mennucci, H. P. Hratchian, J. V. Ortiz, A. F. Izmaylov, J. L. Sonnenberg, D. Williams-Young, F. Ding, F. Lipparini, F. Egidi, J. Goings, B. Peng, A. Petrone, T. Henderson, D. Ranasinghe, V. G. Zakrzewski, J. Gao, N. Rega, G. Zheng, W. Liang, M. Hada, M. Ehara, K. Toyota, R. Fukuda, J. Hasegawa, M. Ishida, T. Nakajima, Y. Honda, O. Kitao, H. Nakai, T. Vreven, K. Throssell, J. A. Montgomery, Jr., J. E. Peralta, F. Ogliaro, M. J. Bearpark, J. J. Heyd, E. N. Brothers, K. N. Kudin, V. N. Staroverov, T. A. Keith, R. Kobayashi, J. Normand, K. Raghavachari, A. P. Rendell, J. C. Burant, S. S. Iyengar, J. Tomasi, M. Cossi, J. M. Millam, M. Klene, C. Adamo, R. Cammi, J. W. Ochterski, R. L. Martin, K. Morokuma, O. Farkas, J. B. Foresman, and D. J. Fox, Gaussian, Inc., Wallingford CT, 2016.
[45] H.J. Berendsen, J.R. Grigera, T.P. Straatsma, The missing term in effective pair potentials, J. Phys. Chem. 91 (1987) 6269–6271. https://doi:10.1021/j100308a038.
[46] C. Caleman, P.J. van Maaren, M. Hong, J.S. Hub, L.T. Costa, D. van der Spoel, Force field Benchmark of organic liquids: density, enthalpy of vaporization, heat capacities, surface tension, isothermal compressibility, volumetric expansion coefficient, and dielectric constant, J. Chem. Theory Comput. 8 (2012) 61–74, https://doi.org/10.1021/ct200731v.
[47] W.L. Jorgensen, D.S. Maxwell, J. Tirado-Rives, Development and testing of the OPLS all-atom force field on conformational energetics and properties of organic liquids, J. Am. Chem. Soc. 118 (1996) 11225–11236, https://doi.org/10.1021/ja9621760.
[48] D. Van Der Spoel, E. Lindahl, B. Hess, G. Groenhof, A.E. Mark, H.J.C. Berendsen, GROMACS: fast, flexible, and free, J. Comput. Chem. 26 (2005) 1701–1718, https://doi.org/10.1002/jcc.20291.
[49] R.E. Stratmann, G.E. Scuseria, M.J. Frisch, An efficient implementation of time-dependent density-functional theory for the calculation of excitation energies of large molecules, J. Chem. Phys. 109 (1998) 8218–8224, https://doi.org/10.1063/1.477483.
[50] N.M. O'Boyle, A.L. Tenderholt, K.M. Langner, cclib: A library for package-independent computational chemistry algorithms, J. Comp. Chem., 29 (2208) 839-845 doi: 10.1002/jcc.20823.